

# THE KEY ROLE OF SNe Ia FOR GALACTIC CHEMICAL EVOLUTION OF p-NUCLEI: 2D - 3D COMPARISON

---

**Claudia Travaglio\***

*INAF-Osservatorio Astrofisico Torino; B2FH Association*

*E-mail: travaglio@oato.inaf.it; claudia.travaglio@b2fh.org*

**F. K. Röpke**

*Universität Würzburg*

**I. R. Seitenzahl**

*Research School of Astronomy and Astrophysics, Mount Stromlo Observatory, Cotter Road,  
Weston Creek, ACT 2611, Australia*

**R. Gallino**

*Dipartimento di Fisica, University of Turin*

**T. Rauscher**

*University of Hertfordshire; Department of Physics, University of Basel*

**W. Hillebrandt**

*Max-Planck-Institut für Astrophysik, Garching bei München*

The bulk of the  $p$ -isotopes is created in the ‘gamma processes’, mainly by sequences of photo-disintegrations and beta decays in explosive conditions in core collapse or in Type Ia supernovae (SNe Ia). We explore single-degenerate SNe Ia in the framework of 2D (DDT-a, Travaglio et al. 2011) and 3D (N100, Seitenzahl et al. 2013) delayed-detonation explosion models. A detailed analysis of the comparison between 2 and 3 dimensions will be presented in this work. Using a Galactic chemical evolution code, we give estimates of the contribution of SNe Ia to the solar  $p$ -process composition (see Travaglio et al. 2014 for a detailed analysis).

*XIII Nuclei in the Cosmos,*

*7-11 July, 2014*

*Debrecen, Hungary*

---

\*Speaker.

## 1. *p*-nucleosynthesis in SNe Ia: 2D and 3D

SNe Ia are associated with thermonuclear explosions of white dwarf (WD) stars that are composed of carbon and oxygen. A ‘classical’ scenario is an explosion triggered once the WD approaches the Chandrasekhar mass. In the *single-degenerate scenario*, which we refer to here, this happens due to accretion of material from a main-sequence or evolved companion star in a binary system. Here, we follow the explosion phase of a Chandrasekhar-mass WD by means of 2-dimensional and 3-dimensional hydrodynamic simulations. For the 2D case we use *DDT-a* (see Travaglio et al. 2011 for details), a delayed detonation model which assumes the WD setup and the deflagration-to-detonation criterion *dc2* of Kasen et al. (2009), i.e. a detonation is triggered at any point of the deflagration flame where a Karlovitz number of  $Ka \geq 250$  is reached and the fuel density is in the range  $0.6 \leq \rho_{\text{fuel}} / (10^7 \text{ g cm}^{-3}) \leq 1.2$ . For the 3D case we use the *N100* model (Seitenzahl et al. 2013), which again has a central density of  $\rho_c = 2.9 \times 10^9 \text{ g cm}^{-3}$ . The initial deflagration is ignited in 100 spherical sparks randomly distributed around the center of the WD. In this particular model, because of the strong deflagration, rather little fuel is burnt during the later detonation phase and the matter distribution does not show large asymmetries.

Detailed nucleosynthesis calculations were performed in post-processing calculations using the tracer particles method. For the 2D model we used 51200 tracers, and 1 million tracers for the 3D model. *p*-process nucleosynthesis occurs in a restricted range of temperature, i.e. from  $1.5 \times 10^9 \text{ K}$  to  $3.7 \times 10^9 \text{ K}$ . We calculate the *p*-process abundances by means of a 1024 species nuclear network. The favourite production mechanism for *p*-process nucleosynthesis is photodisintegration ( $\gamma, n$ ), ( $\gamma, p$ ), and ( $\gamma, \alpha$ ), competing with  $\beta$ -decays. In modeling the SN Ia single-degenerate scenario, we assume that during the accretion phase recurrent flashes have occurred in the He-shell, producing an enhancement of *s*-nuclei that then act as seeds for the *p*-process during the explosion (see Travaglio et al. 2011, 2014 for more details).

In Figure 1 (taken from Travaglio et al. 2011), we show snapshots of the 2D model *DDT-a* at two different times after ignition. On the left side, the hydrodynamic evolution is shown by color coding of the density and the location of the deflagration flame (cyan contour) and the detonation front (blue contour). The plots on the right side show the tracers distribution. The blue, green, and red tracers are in the range of maximum temperature ( $1.5 - 3.7 \times 10^9 \text{ K}$ ) where *p*-process synthesis takes place. From these plots it is evident that the matter undergoing *p*-process nucleosynthesis is almost exclusively heated by the detonation front.

In Figure 2 we show the initial distribution of tracer particles in the 3D model *N100*. With pink, black, and green we coloured the tracers undergoing *p*-process nucleosynthesis, and their colours are for the maximum temperature they reach during the explosion.

One can see that the morphology of the two models is different. The 3D model has multiple ‘fingers’ extending into the star, while the 2D model has a layered, nearly spherical structure and a well defined zone ahead of the deflagration flame. As shown in Figure 2, the deflagration ashes are clearly visible as the hottest material, and the detonation products are the smoothly varying uniform temperature patches. It seems that the ‘fingers’ are connected to the deflagration and that most of the material from these ‘fingers’ is situated up near the tops of the large deflagration plumes. Thus in 3D, because of the existence/persistence of small localized structures, the deflagration continues to burn to lower density along certain directions before being engulfed by the detonation. This

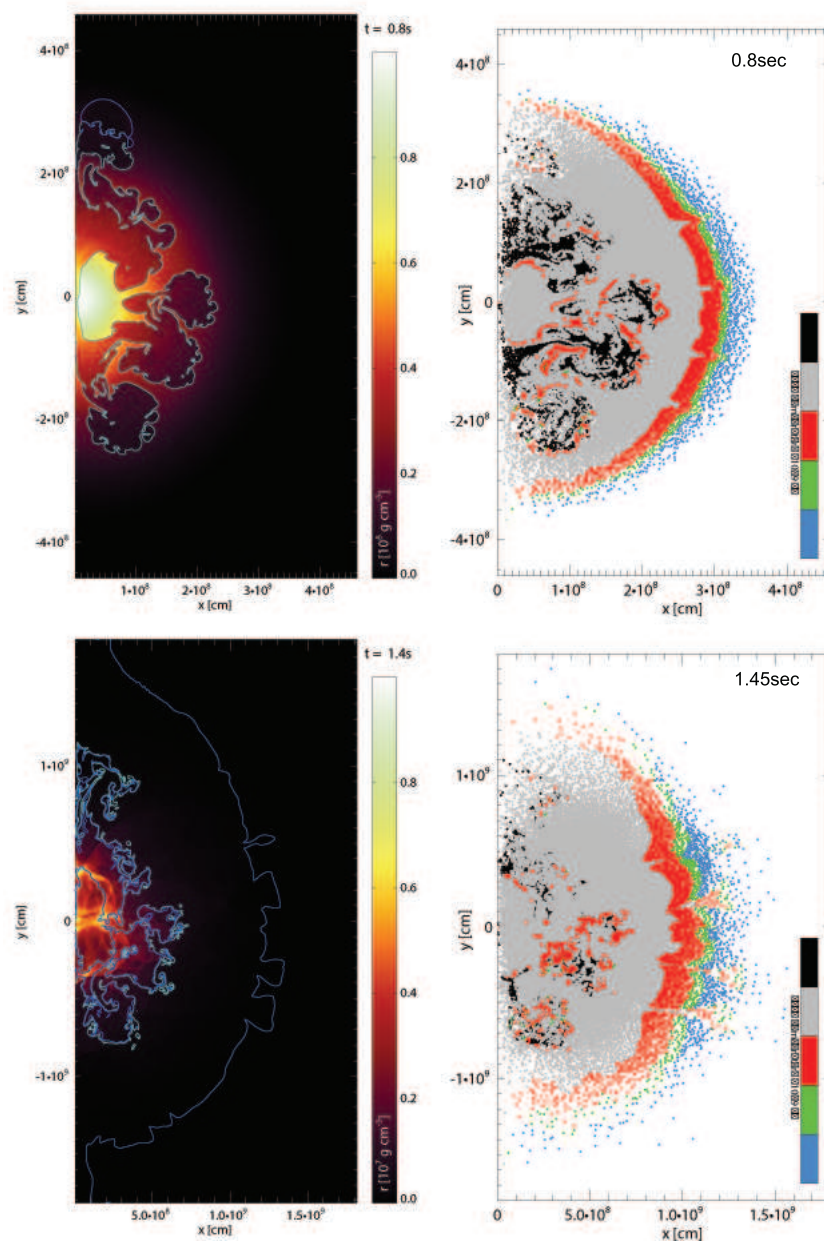


**Figure 1:** Snapshots of the 2D model *DDT-a* 0.8sec and 1.45sec after ignition (Travaglio et al. 2011). On the left the hydrodynamic evolution is illustrated, the density being color-coded. The *cyan contour* indicates the position of the deflagration flame while the *blue contour* shows the detonation front. The right panel displays the distribution of the 51200 tracer particles used in this simulation. Their maximum temperature is color-coded.

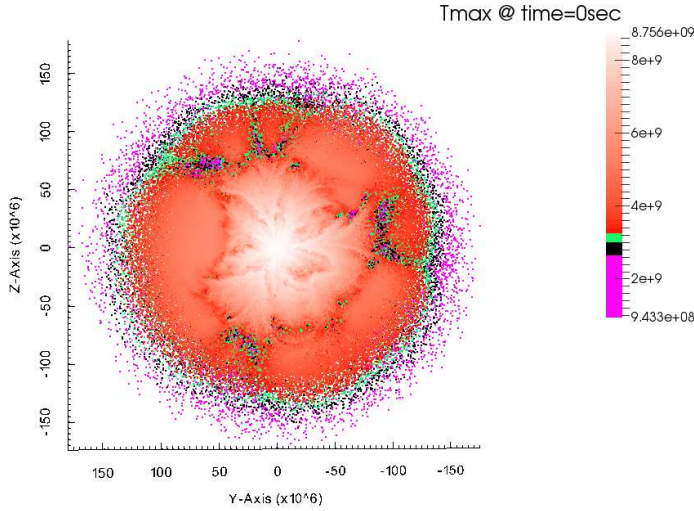


**Figure 2:** Distribution of the 1 million tracers in the 3D model *N100* at the time when the explosion started. The tracers are colored by the maximum temperature reached by each particle during the explosion.

causes a different morphology in 3D as compared to 2D. It should also be noted that due to the axis symmetry the structures seen in Figure 1 are actually ‘rings’ and not ‘blobs’. In conclusion, as far as the *p*-process conditions are concerned, the 3D model has a more complex structure, which cannot be recovered in 2D.

The resulting *p*-process abundances for 2D and 3D are shown in Figure 3, normalized to Fe and to the solar values (from Lodders et al. 2009). The *blue filled squares* and the *red filled circles* are the *p*-only nuclei from  $^{74}\text{Se}$  up to  $^{196}\text{Hg}$ , for 2D and 3D, respectively. As one can see, the resulting nucleosynthesis is very similar in 2D and in 3D, with a few exceptions. The biggest difference shows up in  $^{180}\text{Ta}$  and  $^{138}\text{La}$ , where in 2D the abundances are higher by about a factor of 10. But these are isotopes synthesized at the lowest temperature of all *p*-nuclei, i.e. in the outermost regions of the star, where the 3D model is not very well resolved by tracers. Smaller differences of a factor between 2 and 3, but with the opposite trend (abundances are higher in 3D than in 2D), are seen for  $^{94}\text{Mo}$ ,  $^{113}\text{In}$ ,  $^{115}\text{Sn}$ ,  $^{130,132}\text{Ba}$ ,  $^{136,138}\text{Ce}$ ,  $^{152}\text{Gd}$ , and  $^{156,158}\text{Dy}$ . All these isotopes are mostly produced at a temperature between  $2.6$  and  $2.8 \times 10^9$  K.

Next, we discuss  $^{94}\text{Mo}$  because it is commonly under-produced in models and it is the only light *p*-process nucleus for which 2D and 3D results differ significantly.  $^{94}\text{Mo}$  is synthesized in the outermost layers of the star, both in 2D and 3D, and in the deflagration plumes that continue to burn to low density described above in the 3D model (see also the green tracers plotted in Figure 2). Therefore in 2D  $^{94}\text{Mo}$  is mainly produced in matter that has undergone a detonation, while in 3D it is also made during the later phases of the deflagration. This is likely the cause of the difference between the two models.

Because of a stronger deflagration phase delayed detonation 3D models ‘fainter’ than the one discussed here, i.e. models which less  $^{56}\text{Ni}$  (Seitenzahl et al. 2013), will produce even more  $^{94}\text{Mo}$ . An analysis of the effect of different 3D models with different deflagration strengths is in progress.

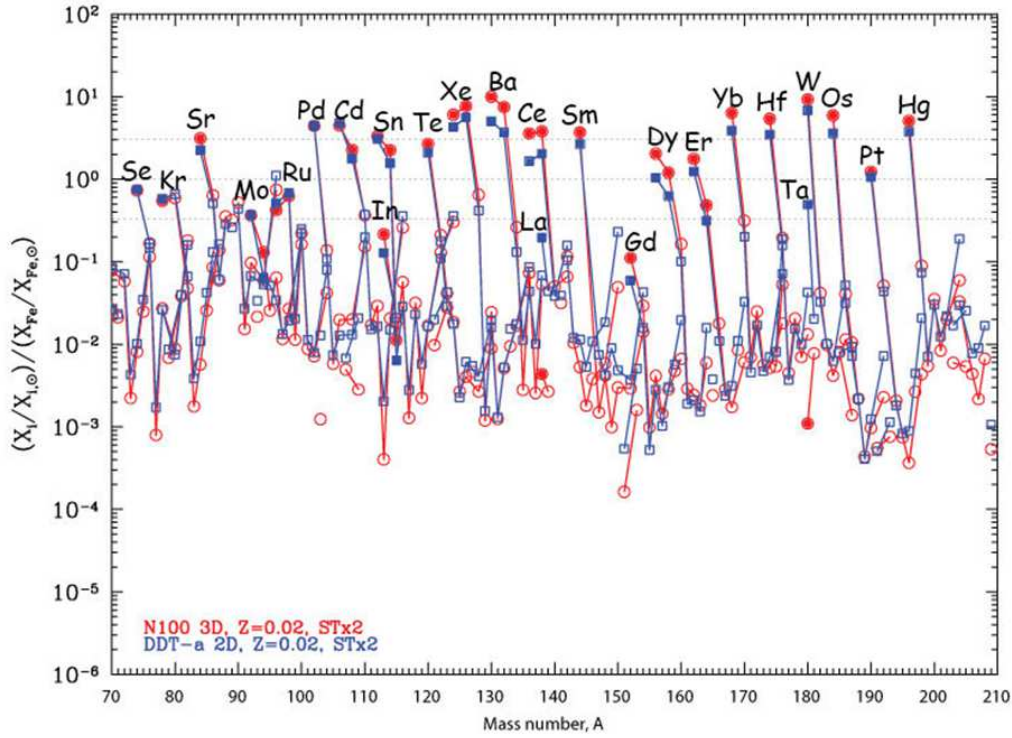


**Figure 3:** *p*-process yields normalized to solar values and to Fe obtained for solar metallicity SN Ia models: DDT-a (blue squares) and N100 (red circles). Filled squares and circles are for *p*-only nuclei.

## 2. Galactic chemical evolution of *p*-nuclei: SN Ia contribution

The Galactic chemical evolution code used here was presented in different works by Travaglio et al. (Travaglio et al. 2004 and references therein). It models the Galaxy as three interconnected zones: halo, thick disk, and thin disk. For the present work we include only SN Ia contributions to the *p*-process (see Travaglio et al. 2014 for more details), but no contributions from core collapse supernovae.

*p*-process nucleosynthesis occurs in SNe Ia starting from a pre-explosion *s*-process enriched seed composition. We considered *s*-seeds at different metallicities in order to model the contribution at different times during the Galaxy evolution. *p*-nucleosynthesis dependence to [Fe/H] (for a detailed discussion we refer to Travaglio et al. (2014).

Assuming that about 70% of all SNe Ia are single-degenerate Chandrasekhar-mass, we find that they produced large amounts of *p*-nuclei in our Galaxy, both the light ones below  $A = 120$  and heavy ones, with almost flat average production factors (within a factor of about 3). Interestingly, Seitzzahl et al. (2013) require a similar fraction ( $\sim 50\%$ ) of Chandrasekhar-mass SN Ia progenitors to explain [Mn/Fe] in the solar neighborhood. Few *special* isotopes like  $^{94}\text{Mo}$  show a behaviour different from the average, possibly connected to SN Ia modeling (as was preliminary discussed in the previous Section). As demonstrated by Travaglio et al. (2014), nuclear physics uncertainties cannot account for the factor of 10 deficiency in  $^{94}\text{Mo}$  abundance relative to the other *p*-isotopes.

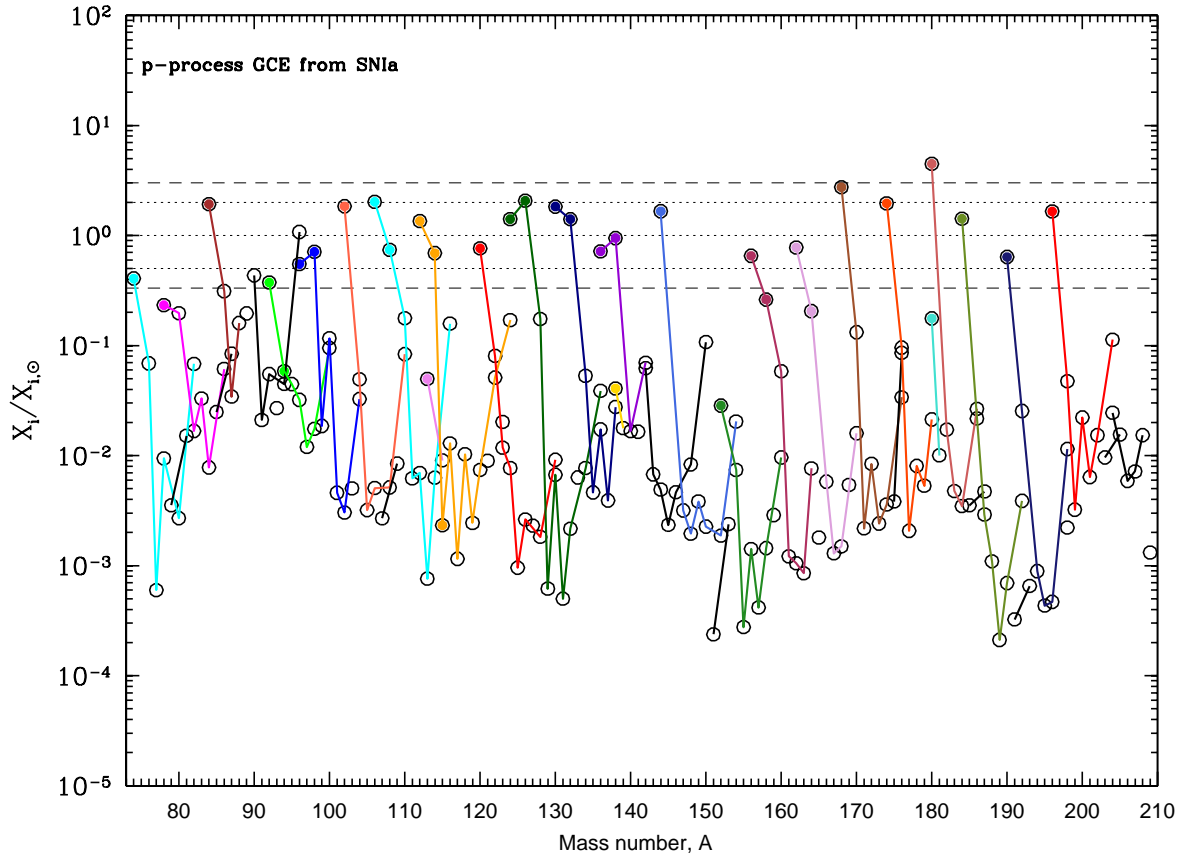


**Figure 4:** Contribution of SNe Ia to the Galactic chemical evolution of *p*-nuclei. Abundances are shown at the time of the Solar System formation. The results were obtained by using our 2D model. Filled dots are the 35 isotopes classically defined as *p*-only.)

### Acknowledgments

This work has been supported by B2FH Association and by the Australian Research Council Laureate Grant FL0992131.

### References

- [1] Kasen, D., Röpke, F. K., & Woosley, S.E. 2009, *Nature*, 460, 869
- [2] Lodders, K. 2009, *ApJ*, 591, 1220
- [3] Seitzzahl, I. R. et al. 2013, *MNRAS*, 429, 1156
- [4] Seitzzahl, I. R., Cescutti, G., Röpke, F. K., Ruiter, A. J., & Pakmor, R. 2013, *A&A*, 559, L5
- [5] Travaglio, C., Gallino, R., Arnone, E., Cowan, J., Jordan, F., & Sneden, C. 2004, *ApJ*, 601, 864
- [6] Travaglio, C., Röpke, F.K., Gallino, R., & Hillebrandt, W. 2011, *ApJ*, 739, 93
- [7] Travaglio, C., Gallino, R., Rauscher, T., Röpke, F. K., & Hillebrandt, W. 2014, *ApJ*, in press